FEDERAL UNIVERSITY OF TECHNOLOGY, AKURE
JOURNAL OF ENGINEERING AND ENGINEERING TECHNOLOGY

CRASHWORTHINESS AND ENERGY ABSORPTION ANALYSIS OF MESOCARP COIR-FIBRE/EPOXY RESIN-REINFORCED GLASS FIBER HYBRID COMPOSITE LAMINATE

Malomo, B. O.

Department of Mechanical Engineering, Obafemi Awolowo University, Ile-Ife,Nigeria

Correspondence: bobmalom@oauife.edu.ng

Maloma B. O. (2023): Crashworthiness and Energy Absorption Analysis of Mesocarp Coir-fibre/epoxy Resin-reinforced Glass Fiber Hybrid Composite Laminate. *Journal of Engineering and Engineering Technology /17(2), 1-18*

Received Date: 10-07-23 **Acceptance Date:15-08-23**

Abstract
Lightweight energy absorbers are increasingly required in state-of the-art automotive applications, but as carbon-fibre reinforced polymers (CFRP) are prohibitive from an economic standpoint, it is critical to develop representative high-performance alternatives. This study focuses on synthesizing coir-fibre/glass fibre reinforced plastic (CF-GFRP) for optimal energy absorption performance. A representative volume element (RVE) model was formulated in DIGIMAT 2017.0 to obtain the elastic properties of the coir-fibre and incorporated in synergy with GFRP by the finite element method (FEM) in ABAQUS v.2018 to obtain the load–displacement response and the crashworthiness properties of the laminated structure. Nine structural representations were specified and investigated according to the influence of loading rate, thickness of GFRP and coir-fibre reinforcement concentration according to the criteria (0.5mm/min, 1mm/min, 1.5 mm/min); (1mm, 1.5mm, 2mm) and (40%, 55%, 70%), respectively. Stress-strain plots indicated that as reinforcement volume fraction increased, there was a modification of the deformation profile to signify the influence of GFRP thickness for prolonged deformation range under stable crushing. Maximum strengths were achieved for consistently thicker GFRP plates irrespective of the concentration volume of fibers. Models that indicated a range 17,000N-22,00N of maximum strength were characterized by a significant capacity to resist inhomogeneous deformation due to enhanced period of densification after progressive crushing. Variations in maximum crushing force F_{max} was found to be significant and geometrically-sensitive with high values indicated for models under higher loading rates. The energy absorbed (EA) was significant for models that indicated high resistance to peak loads and also those that indicated smoother load-unloading profiles. The specific energy absorbed (SEA) and crush force efficiency (CFE) increased with increasing GFRP thickness for a given reinforcement concentration across the models. The best structural configuration for energy absorption was found by Pareto characterization as experimental validation was found to be consistent with simulated FEM results in establishing the crashworthiness potential of the laminated composite.

Keywords: *Coir-fibre, deformation, energy absorption, structural models*

Introduction

The need to develop cutting edge light-weight structures, devices and high performance systems is paramount to the material world as it continues to grapple with the stringent demands of the mechanical industry, in recognition and response to a plethora of socio-economic and environmental challenges associated with the efficient utilization of resources and in maximizing the useful potentials of raw materials in various applications (Baroutaji *et al*., 2017; Essabir *et al*., 2016; Beardmore and Johnson, 1986). It is well-understood that material behavior is central to the ultimate performance of structures, hence there is now a strong emphasis to advance material-based protocols in developing state-of-the-art material forms capable of providing an improvement and ensuring the preservation of notable performance characteristics, such as the stiffness, dimensional stability, corrosion resistance and impact resistance, etc. To this end, hybrid composites and other carefully-engineered material forms synthesized through unconventional and advanced processes are candidates to replace traditional monolithic materials for superior performance in the automotive and aerospace manufacturing industries; where there is now a growing demand for glass and carbon-fibre reinforced polymers, particle-reinforced metallic systems, advanced high strength steels (AHSS), etc., to replace cast iron and steels. These materials are known to be consistent in their behaviour and are suitable for application in the

design of light-weight, structurally-tough components, critical to achieving the goal of fuel efficiency, safety and enhanced overall system performance (Beardmore and Johnson, 1986; Supian *et al.*, 2019; Albahash and Ansari, 2017).

Invariably, one of the most strategic and critical performance criteria in the automotive industry is occupant safety, which is a driver of cut-throat competition among automakers. Consequently, to achieve the much-required competitive edge has been largely predicated on evolving a superior crashworthiness performance based on the effective incorporation of advanced mechanisms to modulate damage development and progression under impact for optimum crash protection. Therefore, in recent times, a thrust of research efforts has been devoted to optimizing the energy absorption efficiencies of related systems and structures following the profound pioneering work of Weirzbicki and Abramowicz, (Weirzbicki and Abramowicz, 1983; Abramowicz and Jones, 1986) who jointly postulated the super folding element (SFE) theory to describe the relationships between deformation mechanisms and energy absorption criteria. Their study has facilitated the development of thin-walled metallic structures that have found wide applicability in safety designs over the decades, based on the premise that the mechanisms for the dissipation of kinetic energy in crash situations in high-speed transportation can easily follow a predictable and controllable scenario, tailorable for best performance. However, one of the major drawbacks associated with the exploitation of metallic structures is the challenge to evolve a light weight absorber characterized by a high specific energy absorption (SEA) factor (Abolfathi and Nia, 2018; Wu and Zhi, 2020), which is a foremost necessity in safety designs for modern transportation systems. In light of this, the quest for light-weight structures in certain automotive applications has intensified, with a growing interest in fiber-reinforced polymeric (FRP) composites (Baroutaji *et al*., 2017; Supian *et al*., 2019). This is not only to harness their excellent mechanical properties and weight reduction attributes, but because of the need to fully understand the complexities associated with the deformation and dissipation of crush energy by FRP's occurring by the virtue of a myriad of failure criteria, such as; fiber breakage, matrix cracking, delamination or a combination of these, through which it would be feasible to closely control the mechanisms for energy absorption.

FRP's have been mostly hybridized with metals to achieve a good compromise in specific strength and modulus for certain applications, especially shell structures and thin tubular sections; and they have demonstrated profound energy absorption performances. For instance, the authors (Sun *et al.*, 2018) investigated the quasi-static axial crushing behavior of hybrid wrapped carbon fibre reinforced polymer (CFRP) and square aluminum tubes in order to evaluate the inference of ply orientations, and they found that the performances of the hybrid tubes were superior to those of the aluminum tubes. The performance of fibre-reinforced composite steel tubes under axial impact have been investigated based on the geometric features of various GFRP thicknesses, winding angles and steel tube diameters in a robust and optimized parametric evaluation scheme for energy absorption (Cai *et al.*, 2016). The crashworthiness of a vehicle energy absorber has been studied based on a hybrid square hollow steel tube filled with glass-fiber reinforced 'polyamide 66' honeycomb structure (Paz *et al.*, 2014). Furthermore, to address the scenarios of oblique collisions in crashes, the authors investigated the ultimate bending moments and energy-absorption performance of aluminum/GFRP hybrid tube beams with emphasis on the effects of thin GFRP skin layer in relation to bending deformation behavior and fracture characteristics and they found the optimal thickness and layup of the composite skin layer consistent with the best performance of the hybrid tubes (Jung *et al.,* 2009). Besides metal-hybrids with FRP's, an effective amalgamation of FRP's with synthetic fibres have also been achieved for similar strategic purposes. The effect of geometry and energy absorption of square cross section, graphite/epoxy and Kevlar/epoxy tubes under static crushing has been investigated in which the effect of decreasing width-wall thickness (b/t) ratio was correlated with increasing energy absorption (Pickett and Dayal, 2012; Liu *et al*., 2019; Farley, 1987). Related studies have also been conducted to quantify the oblique lateral crushing characteristics of thin-walled circular GFRP and CFRP tubes (Sun *et al*., 2020; Xiang, *et al*., 2018). The crashworthiness properties of quasi-unidirectional E-glass/polyester semi-hexagonal composite structures for automotive crash applications have also been studied to evaluate the effect of manufacturing processes based on the interlaminar shear strength response and the specific energy absorption (SEA) capability (Issac, and Ezekwem, 2021). In the same vein, the impact resistance of preloaded E-glass fibre/polyester plain weave laminate composite plates have been studied (Esnaola, *et al*., 2016), and a correlation of biaxial loading with ballistic limit performance was presented.

Thus far, FRP's have demonstrated exceptional properties on energy absorption as compared with metals and are preferred candidates in motorsport applications. However, the prohibitive costs of synthetic fibres (carbon-fibre, kevlar, aramid, etc,.) along with the growing environmental concerns on recyclability, invigorates the need for technologically-viable alternatives. In this purview, it has been reported that by incorporating natural fibres as fillers or second phase materials in developing hybrid composites can provide promising and desirable results. Specifically, some natural fibers such as jute, hemp, sisal, kenaf, coir,

flax, banana etc., have been shown to exhibit mechanical properties comparable to glass fibers [Jawaid *et al*., 2019; Pickering *et al*., 2016). This quality, coupled with their low densities, biodegradability, renewability, availability and low costs, make them directly applicable in lightweight, cost-effective automotive applications. Therefore, in line with the requirements of crash safety, hybrid natural fibre based FRP's have been investigated on their impact performances. For instance, the authors (Safri *et al*., 2017) have demonstrated that a hybrid composite laminate of banana/E-glass fabrics reinforced polyester could possess a considerable impact resistance; also a hybridization mechanism to enhance the impact strength of jute/glass and jute/carbon-reinforced composites has been postulated (Pickering et al, 2016; Safri *et al*., 2017), similarly, the post-impact behavior and damage tolerance capability of hemp-based FRP have been studied to determine the hybridization effect of basalt fiber additions (Jawaid *et al*., 2019). Furthermore, the crashworthiness of thin-walled E-glass fibre/epoxy resin reinforced (GFRP) composite conical frusta has been investigated to determine the influence of ply orientation and the laminate wall thickness on energy absorbing capability (Kathiresan *et al*., 2014). From the foregoing, the hybridization concept is very significant in improving the overall performance of composites as it provides a material design engineer the flexibility to tailor best properties of the constituents (Jawaid *et al*., 2019; Sebaey *et al*., 2023). Consequently, from this standpoint and based on the understanding that composite laminates are now replacing conventional metals in automotive applications, this current work draws its motivation. The research focus is to investigate the hybridization effect of the inexpensive, naturally-occurring coir-fibre with the high strength synthetic glass fibre on energy absorption performance taking into consideration, the variations in the concentration of the coir-fibre and thickness of the glass fiber sheets, towards evolving an FRP hybrid composite suitable for adoption in automotive applications.

Crashworthiness criteria

The energy performance parameters are obtained from crash load-displacement curves and can be described by the following properties (Xiang *et al*., 2018, Sun *et al*., 2020).

(i) The peak Crush Force (PCF):

The peak crush force is observed at the early stage of the crushing process before the plateau region is reached in the stress-strain curve is attained.

(ii) Energy Absorption (EA):

This property is the total strain energy absorbed during the plastic deformation and it is a measure of the work done by the crush force. It is given mathematically by Equation (1);

$$EA = \int_0^{\delta_{max}} F(\delta)d\delta \quad (1)$$

where $F(\delta)$ is the crushing force related to the displacement δ and δ_{max} is the effective maximum displacement.

(iii) Specific Energy Absorption SEA:

This is the measure of the absorbed energy per its unit mass, during the crushing process and it is given by Equation (2);

$$SEA = \frac{EA(\delta)}{d} \quad (2)$$

(iv) The mean crush force (F_{av}):

This is the average compressive force exerted on the structure over the entire crushing distance δ_{max} and it is given by Equation (3);

$$F_{av} = \frac{EA(\delta)}{\delta_{max}} = \frac{\int_0^{\delta max} F(\delta)d\delta}{\delta_{max}} \quad (3)$$

(v) Crush force efficiency CFE:

This is the ratio of the mean crush force (MCF) to the peak crush force (P_{max}). It is an important crashworthiness parameter to evaluate structures of varying masses and geometries. It is given mathematically by Equation (4);

$$CFE = \frac{MCF}{P_{max}} \quad (4)$$

Finite Element Modelling

Composite Material Specifications

The hybrid polymer composite structure consists of a primary (naturally-occuring, coir fibre) and secondary (synthetic glass fibre) reinforcements in combination with an epoxy-resin matrix. The coir-fibre is a biodegradable natural lignocellulosic filler derived from coconut palm (Cocosnucifera) as shown in Figure 1, and it is a representative alternative to the expensive carbon and glass fibres in reinforcing polymers (Sengupta and Basu, 2016). GFRP is essentially a strong, lightweight material composed of a plastic matrix reinforced with fibers of glass. It is generally less expensive and less brittle than carbon fiber and possesses good mechanical properties (Cai *et al*., 2016). Its bulk strength is comparable to those of metals and easily amenable to mass production

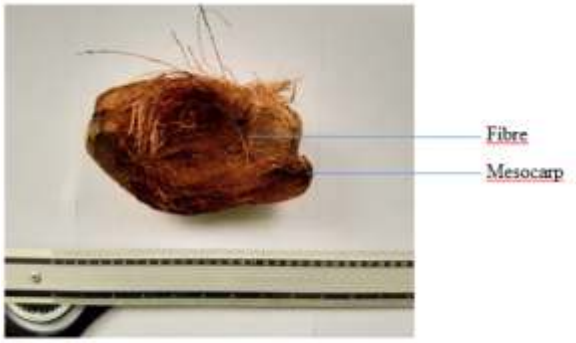

Figure1: Coconut palm fruit structure

.The stiffness and strength of coir fiber is generally lower than that of the synthetic glass fiber, but by virtue of its lower density, the specific properties are comparable. It is expected that the overall properties of the hybrid composite would be enhanced through the mechanism of load transfer from the epoxy resin matrix to the reinforcing fibres (Jung *et al*., 2009). For the model description, the coir is constituted by continuous fibres with high aspect ratio, corresponding to a length-to-diameter (L/D) ratio that is infinitely large which is a reasonable approximation consistent with the development of stiff and strong fibers that are flexible for large scale production in automotive light load-bearing applications. The GFRP is modelled as an embodiment of layered thin lamina consisting of parallel interlaced fibres that are equal in number in both their in-plane perpendicular directions where the major requirement is to evaluate the effect of the laminate thicknesses. The physical properties of the coir fibre, glass fibre and epoxy resin (LY556) are shown in Table 1.

Table 1: Baseline physical properties of coir fibre, GFRP and epoxy

Material	Tensile strength (MPa)	[illegible]	Elongation at break (%)	Density (g/cm^3)	Ref.
Coir fibre [30]	220	6	15-25	1.25	[30]
Glass fibre	4400	90	4.5	2.48	[33]
Epoxy (HY655)	31	3.7	-	1.15	[32]

Model geometry and characteristics

A fully three-dimensional model was developed to characterize the response of the hybrid composite under quasi-static compression is shown in Figure 2. The parameters considered for modelling the structure are the thickness of the glass fibre specified at three levels of 1.0, 1.5 and 2.0 mm; the filler concentration at 40%, 55% and 70%; and the load-deformation rate of the composite at 0.5, 1.0 and 1.5 mm/min. A parametric simulation study to investigate the mechanical response resulting from the combination of the design factors was formulated based on the Taguchi's matrix orthogonal array (Alshahrani *et al*., 2022) as shown in Table 2. Herein, a total of 9 structural configurations were described.

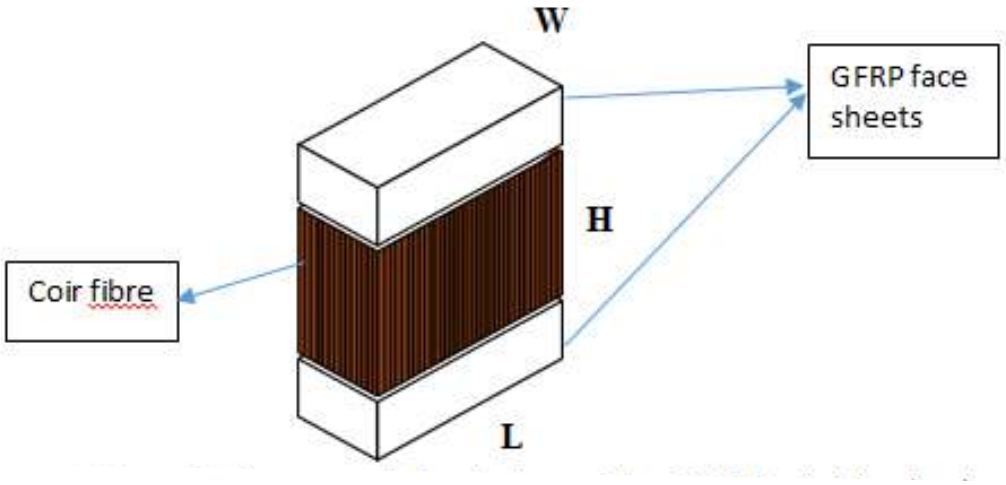

Figure 2: Conceptual description of the GFRP/coir fibre laminate

Table 2: Matrix design layout

Model	Loading rate (mm/min)	Thickness layer (mm)	Fiber concentration (%)
1	0.5	1	40
2	0.5	1.5	55
3	0.5	2	70
4	1	1	55
5	1	1.5	70
6	1	2	40
7	1.5	1	70
8	1.5	1.5	40
9	1.5	2	55

Material Constitutive Model

The failure of the GFRP/Coir fibre hybrid fibre reinforced laminate can be initiated according to the Hashin's damage law when any of the following four failure modes of fiber tension (F_t), fibre compression (F_c), matrix tension (F_{mt}) and matrix compression (F_{mc}) given in Equations (5-9) has a value that is equal or greater than unity (Hashin, 1980).

$$F_t = \left[\frac{\widehat{\sigma_{11}}}{X_T}\right]^2 + \left[\frac{\widehat{\sigma_{12}}}{S_L}\right]^2 = 1 \quad (5)$$

$$F_C = \left[\frac{\widehat{\sigma_{11}}}{X_C}\right]^2 = 1 \quad (6)$$

$$F_{tm} = \left[\frac{\widehat{\sigma_{22}}}{Y_T}\right]^2 + \left[\frac{\widehat{\sigma_{12}}}{S_L}\right]^2 = 1 \quad (7)$$

$$F_{cm} = \left[\frac{\widehat{\sigma_{22}}}{2S_T}\right]^2 + \left(\left[\frac{Y_C}{2S_T}\right]^2 - 1\right)\left[\frac{\widehat{\sigma_{22}}}{Y_C}\right]^2 \quad (8)$$

where the effective stress tensor σ_{ij} is represented by components $\widehat{\sigma_{11}}$ and $\widehat{\sigma_{22}}$ corresponding to stresses in the fibre and normal to the fibre directions respectively. X_T and X_C, are the fibre tensile and fibre compressive stresses; Y_T, and Y_C are the matrix tensile and matrix compressive stresses; while S_L and S_T are the longitudinal and transverse shear strengths respectively. This failure criteria holistically satisfies the conditions for intralaminar damage (fiber breakage and matrix cracking).

To establish the conditions for the interlaminar failure (delamination), the constitutive equations of the form in Equation (9) is presented;

$$\sigma = A_{dm}\varepsilon \quad (9)$$

where σ, ε are the stress and strain components while A_{dm} is the stiffness matrix expressed in terms of damage degradation by Equation (10);

$$A_{dm} = \frac{1}{D}\begin{bmatrix} (1-d_f)E_{11} & (1-d_f)(1-d_m)\nu_{21}E_{11} & 0 \\ (1-d_f)(1-d_m)\nu_{12}E_{22} & (1-d_m)E_{22} & 0 \\ 0 & 0 & D(1-d_s)G_{12} \end{bmatrix} \quad (10)$$

where the damage variables d_f, d_m and d_s represent the tension, compression and shear failures respectively. The scalar damage parameter D reflects the degradation of material stiffness according to the expression given by Equation (11);

$$\boldsymbol{D} = 1-(1-d_f)(1-d_m)\nu_{12}\nu_{21} \quad (11)$$

The failure initiation criteria is satisfied by the damage evolution factor $\boldsymbol{D}$ that ranges from 0 (undamaged) to 1 (fully damaged) to characterize the degradation of material stiffness.

The delamination that occurs between different GFRP lamina and coir fibres is analyzed by the cohesive zone (CZM) model according to the quadratic loss function given by Equation (12) (Camanho *et al.*, 2002);

$$\left\{\frac{\langle\tau_n\rangle}{\tau_n^0}\right\}^2+\left\{\frac{\langle\tau_s\rangle}{\tau_s^0}\right\}^2+\left\{\frac{\langle\tau_t\rangle}{\tau_t^0}\right\}^2=1 \quad (12)$$

where, t_n^0, t_s^0, t_t^0 are the peak values of the nominal stress components across the interface and damage is assumed to occur when the nominal stress ratios attains a value of 1.
The stress components are related to the damage according to the following expressions in Equations (13-14);

$$\begin{cases}(1-D)\tau_n & \overline{\tau_n}\geq 0\\ \overline{\tau_n} & \text{otherwise}\end{cases} \quad (13)$$

$$\tau_s=(1-D)\overline{\tau_s} \quad (14)$$
$$\tau_t=(1-D)\overline{\tau_t}$$

The failure initiation displacements U_n^0 and U_s^0, in terms of surface tractions can be expressed as follows in Equation (15):

$$U_n^0={}^{\sigma_n}/_{E_f};\qquad U_s^0={}^{\sigma_s}/_{E_f} \quad (15)$$

where, σ_n, σ_s, E_f, are the interfacial normal compressive strength, shear strengths and stiffness. respectively.
The final displacements U_n^1 and U_s^1 are obtained from the fracture toughness G_n for the normal mode and critical energy release G_s for the shear mode tractions by Equation (16):

$$U_n^*={}^{2G_n}/_{\sigma_n}\qquad U_s^*={}^{2G_s}/_{\sigma_s} \quad (16)$$

The effective separation displacement δ_m for the normal and shear separations is given by Equation (17);

while, the mixed-mode damage initiation criteria δ_m^0 is expressed by Equations (18-19);

$$\delta_m^0=U_n^0\times U_s^0\times\sqrt{\frac{1+\beta^2}{U_s^{0^2}+(\beta\times U_n^0)^2}} \quad (18)$$

Where $\beta=\frac{U_s}{U_n}$ (19)

The total separation by mixed-mode failure is then captured by the Benzeggagh-Kenane (B-K) criterion in Equation (20);

$$\delta_m^f=\frac{2}{E_p\times\delta_m^0}[G_n+(G_s-G_n)]\times\left(\frac{\beta^2}{1+\beta^2}\right)^{\gamma} \quad (20)$$

where γ is the (B-K) criterion exponent.
The damage evolution variable D is expressed in terms of the maximum mixed-mode displacement, δ_{max}, according to Equation (21);

$$D=\frac{\delta_m^f\times(\delta_{max}-\delta_m^0}{\delta_{max}\times\left(\delta_m^f-\delta_m^0\right)} \quad (21)$$

Numerical Implementation
Representative Volume Element (RVE) Homogenization

To analyze composite structures, a common practice is to incorporate effective or homogenized material properties to circumvent the complexities of accounting for the effects of individual phases and geometrical constraints. In most cases, these effective properties are difficult to measure prompting the need for numerical homogenization. The elastic properties and strength parameters of GFRP/epoxy and Coir fibre/epoxy are required for the Hashin's progressive damage model and analysis of the hybrid composite laminate, however while the former is readily available in the open literature as presented in Table 3 (Abood *et al.*, 2021), the latter must be found by a homogenization scheme and in this case, the Mori-Tanaka/Eshelby mean field theory was implemented in the DIGIMAT software environment. From thence, the effective elastic moduli viz; longitudinal modulus *E11,* transverse modulus *E22*, longitudinal shear modulus, *G12,* transverse shear modulus *G23*, and major Poisson's ratio

Table 3: Elastic and strength properties of GFRP

Property	Description	Value
E_{11}	Young's modulus in longitudinal (fibre) direction (GPa)	48
E_{22}	Young's modulus in transverse direction (GPa)	12
G_{12}	In-plane shear modulus (GPa)	6
G_{23}	Out of plane shear modulus (GPa)	
v_{12}	Major Poisson ratio	0.28
X_T	Longitudinal tensile strength (MPa)	1200
X_C	Longitudinal compressive strength (MPa)	800
Y_T	Transverse tensile strength (MPa)	59
Y_C	Transverse compressive strength (MPa)	128
S	Shear strength (MPa)	25

$$\sigma_m = \sigma_0 + E_m\bar{e} = E_m e^0 + E_m\bar{e} \quad (23)$$

where, σ_0 is the external stress applied to the composite, E_m, e^0 and $\bar{e}$ are the stiffness tensor, the mean strain of the matrix and the eigenstrain or disturbance strain in the matrix due to the fibers. The constrained strain in the fibres and the mismatch strain between the matrix and the fibres are given e_f^c and e_f^T respectively. The stiffness tensor of the composite C_s is expressed via the relations in Equation (24-26);

$$E_s^{-1} = [I + fB(I + Q)]E_m^{-1} \quad (24)$$

Where, $B = \left((E_f - E_m)S + E_m^{-1}\right)(E_f - E_m)$ (25)

$$Q = (I + f(S - I)B)^{-1}(-f(S - I)B) \quad (26)$$

E_f, f, S and I are the stiffness tensor of fiber, fiber volume fraction, Eshelby tensor and identity tensor, respectively.

In DIGIMAT, the boundary value problem on the representative volume element (RVE) structure of the epoxy/coir fiber composite (Figure 3) developed by the random sequential adsorption method (RSA) (Zhang *et al*., 2016) is solved by substituting the elastic modulus and Poisson's ratio of the epoxy matrix and coir fibres into Equation (24) to generate a homogenized and stress-strain response which determines the effective elastic moduli of the composite.

Structural Modelling

Numerical analysis was performed on the three-dimensional model (Fig.4) using the commercial finite element analysis (FEA) software, ABAQUS/Explicit (Omairey *et al*., 2018) to predict the load-deformation behaviour, obtain the corresponding deformation profiles and determine the crashworthiness properties by incorporating the progressive damage model of Hashin's intralaminar and interlaminar damage initiation and evolution criteria. The model as shown in Figure 4, illustrates the action of axial loads on the deformable coir/GFRP structure. To prevent the initial penetration of the top GFRP layer and the deformable structure, a minimum clearance 0f 0.001mm was applied between the assemblies. A tangential behavior, 'surface-to-surface' contact condition was used to describe the interacting contacting surfaces with a penalty frictional formulation of 0.2. The top surface of the rigid bottom plate and the bottom face of the deformable structure are coupled by the 'node-to-surface' interaction criterion and the lateral motion of the contact was prevented by the 'rough' frictional contact condition. The deformable structure was discretized by the shell element 'S4R' with three integration points. A mesh size of 2mm with control condition of ($0.0 < \min < 1.0$) implemented through the reduced integration and hourglass control was considered appropriate to modulate the sensitivity response of the elements such that the ratio of the artificial energy to the internal energy is less than 5% in order to accurately capture the collapse response of the structure. Consequently, the material properties for the homogenized coir-fiber/epoxy and GFRP/epoxy systems were incorporated to

the deformable shell structure using the composite lay-up function in ABAQUS. The load application was performed by imposing an axial load of 100 N directly from the top plate with a velocity of 0.5 mm/min. The effective crushing distance is set at 20 mm which is about 67% of the total length of the overall assembly, a conceptual idea in tandem with the recommendations of the authors

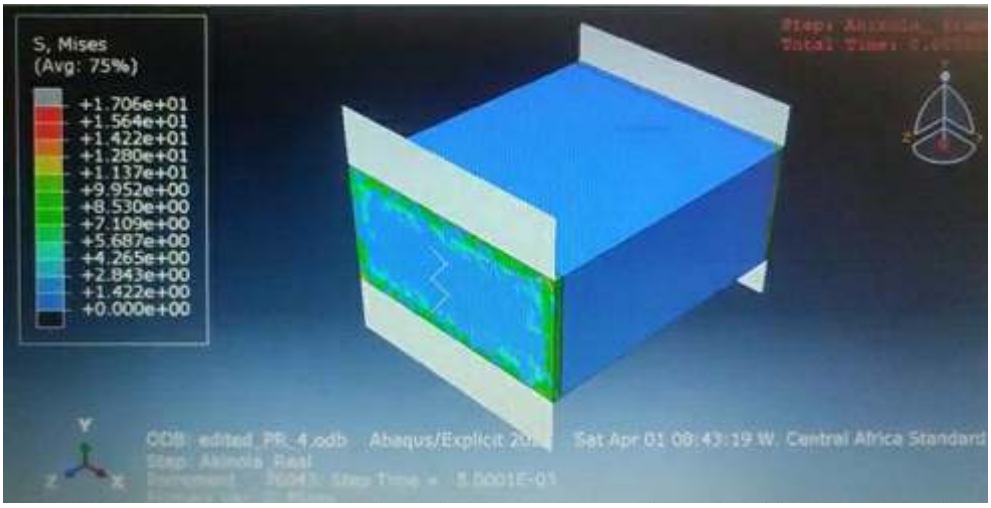

Figure 4: Model analysis by the finite element method in ABAQUS

(Baykasoglu and Baykasoglu, 2017). The explicit dynamic solver was implemented with a time step of 5 milliseconds to capture the quasi-static displacement condition as the interface force progressively contacts the deformable structure through the entire loading history.

Experimental validation

Samples of coconut palm fruit which are about 8 months old, were obtained from the Nigerian Oil palm Research Institute (NIFOR), Lagos. The coconut fruit shell is composed of three layers, namely; the outer exocarp, the porous, fibrous mesocarp and the inner hard endocarp as shown in Fig.1. The mesocarp is of utmost interest to the study as it is the direct parent material of the coir fibres. The coconut shells were split up and dried in sunlight for 2 weeks to get rid of the moisture and then subjected to heat treatment at 90^0C until a moisture content of 8.8% was achieved, a value considered appropriate for well-seasoned dry shells (Sengupta and Basu, 2016). The shells were cut into samples according to the dimensions 23.25 mm x 12.00 mm x 31.75 mm (*L x W x H*) as shown conceptually with the GFRP face sheets in Figure 2. Since the mesocarp is composed of the coir fiber, coir dust and void, adequate weight measurements according to ASTM D3800-M-11 based on the Archimedes principle was applied to calculate the volume fractions of fibres, according to the expression given by Equation (27);

$$\rho_f = \frac{\rho_b W_{f\,a}}{W_{f\,a} - W_{f\,b}} \qquad (27)$$

where ρ_b is the density of benzene, while $W_{f\,a}$ and $W_{f\,b}$ are the weights of mesocarp in air and liquid benzene respectively. The void content was determined according to ASTM D2734 standard by Equation (28):

$$void\ content\,(\%) = \frac{\rho_{theoretical} - \rho_{experimental}}{\rho_{theoretical}} \qquad (28)$$

Results and Discussion

Load-deformation plots

The stress-strain behavior of the composites is indicated by the plots in Figures (5-7). Models (1-3) are presented in Figure 5, models (4-6) in Figure 6 and models (7-9) in Figure 7. In general, at 40% fiber concentration regardless of the thickness of the GFRP sheets, the deformation history is very consistent where-in a range of 850-900 N of force was attained at the elastic domain within the same deformation range.

This was followed by a period of monotonic progressive crushing and a sudden collapse. As the reinforcement volume fraction increased to 55%, there was a change in the deformation profile, even though the initial peak forces that characterized the onset of instability occurred at the same stress as compared with the 40% models, this effect may be attributed to the influence of GFRP thickness which is apparent by virtue of the prolonged deformation range in which more energy is absorbed under stable crushing. In this process, relative to the 40% configurations, the deformation range increased by 15 mm and with the maximum strength being attained at approximately 6000 N. As indicated in Figure 9 The variations in the thickness of the GFRP indicated a significant influence on the character of the 55% reinforcement curves where the maximum stresses increased with thicknesses to suggest that the energy absorption performance is underscored by enhanced load-bearing effect. However, the fact that the deformation range remained consistent as thicknesses evolved showed that the phenomenon of load transfer by the mesocarp fiber was unaltered by increasing GFRP thickness. With regard to specimens with 70% mesocarp fiber reinforcement, it was surprising to note that, the initial peak stresses also corresponded to the magnitudes found in the 40% and 55% models which is an effect that reasonably justifies that the elastic deformation domain is not sensitive to increment in reinforcement concentration, even though there is a significant change in the entire deformation profile. Accordingly, as indicated in Figs 8-10. The maximum strength of the 70% models was found to vary between 17,000 N -22,000 N which represents a significant rise in the capacity to resist inhomogeneous deformation due to an enhanced period of densification after progressive crushing. The effect of varying the thickness of the GFRP sheets was also significant as indicated by sudden variations in peak stresses attained after densification. Thus, it follows that the properties of natural fiber reinforced composites can be improved by hybridizing with high strength synthetic fibers.

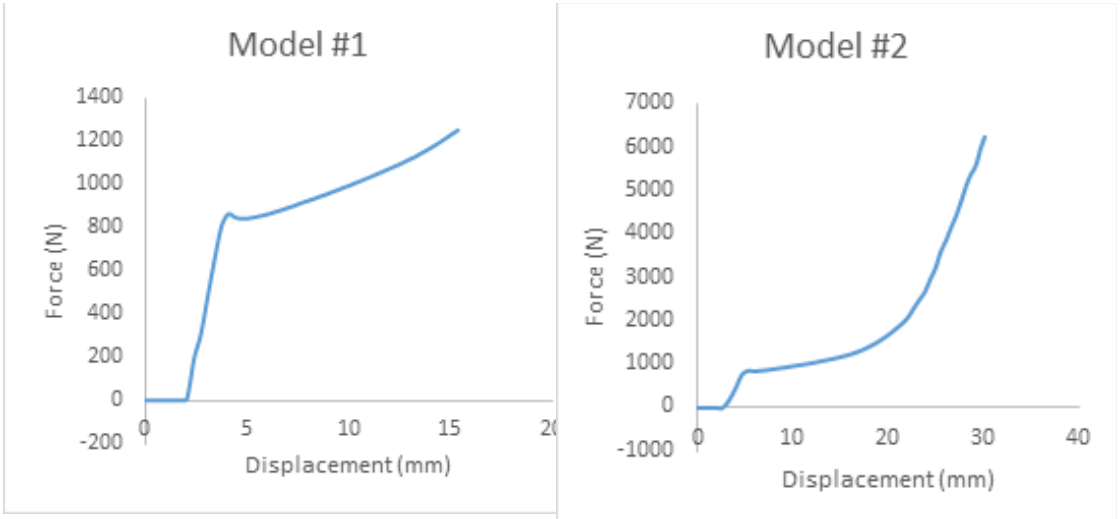

(a)

(b)

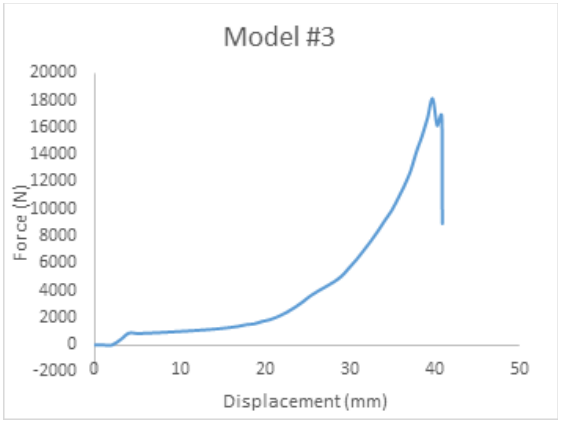

(c)

Figure 5: Load-displacement curves (a) Model 1 (b) Model 2 (c) Model 3

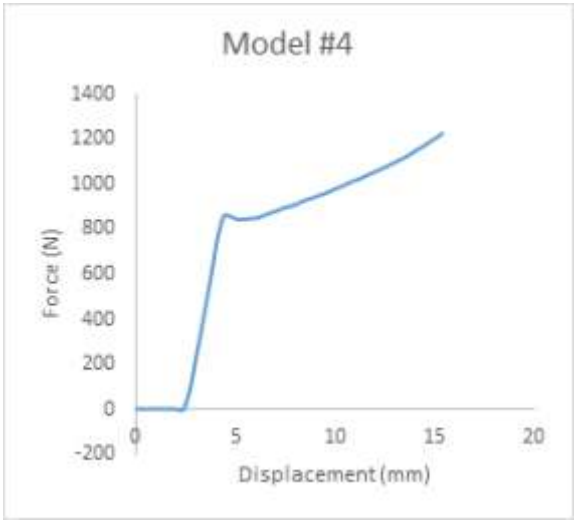

(a)

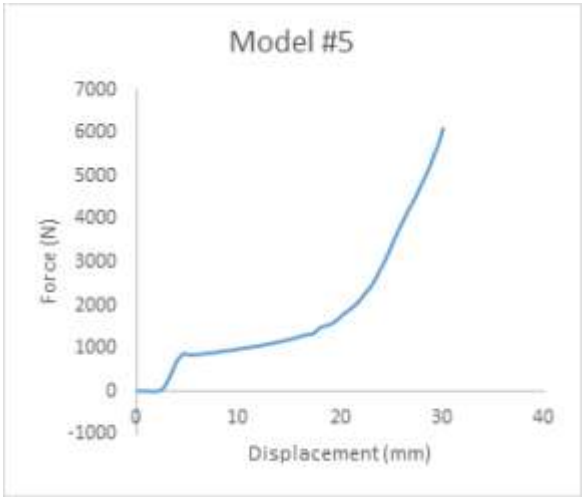

(b)

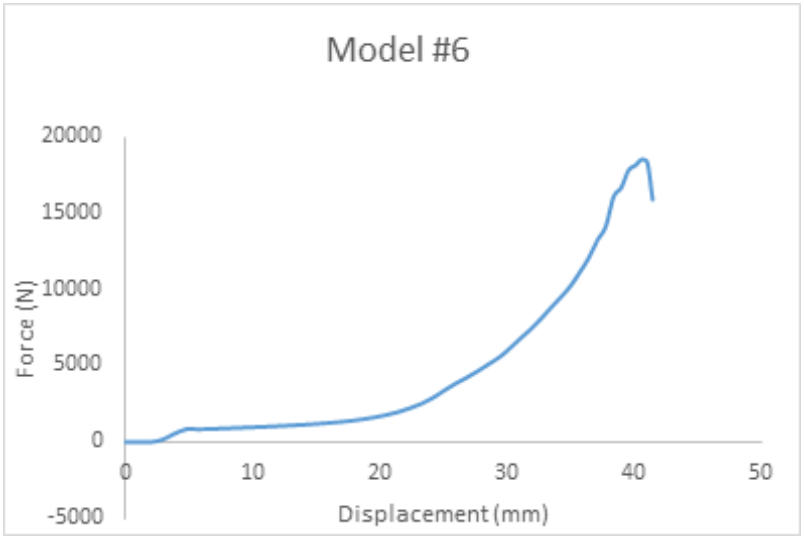

©

Figure 6: Load-displacement curves (a) Model 4 (b) Model 5 (c) Model 6

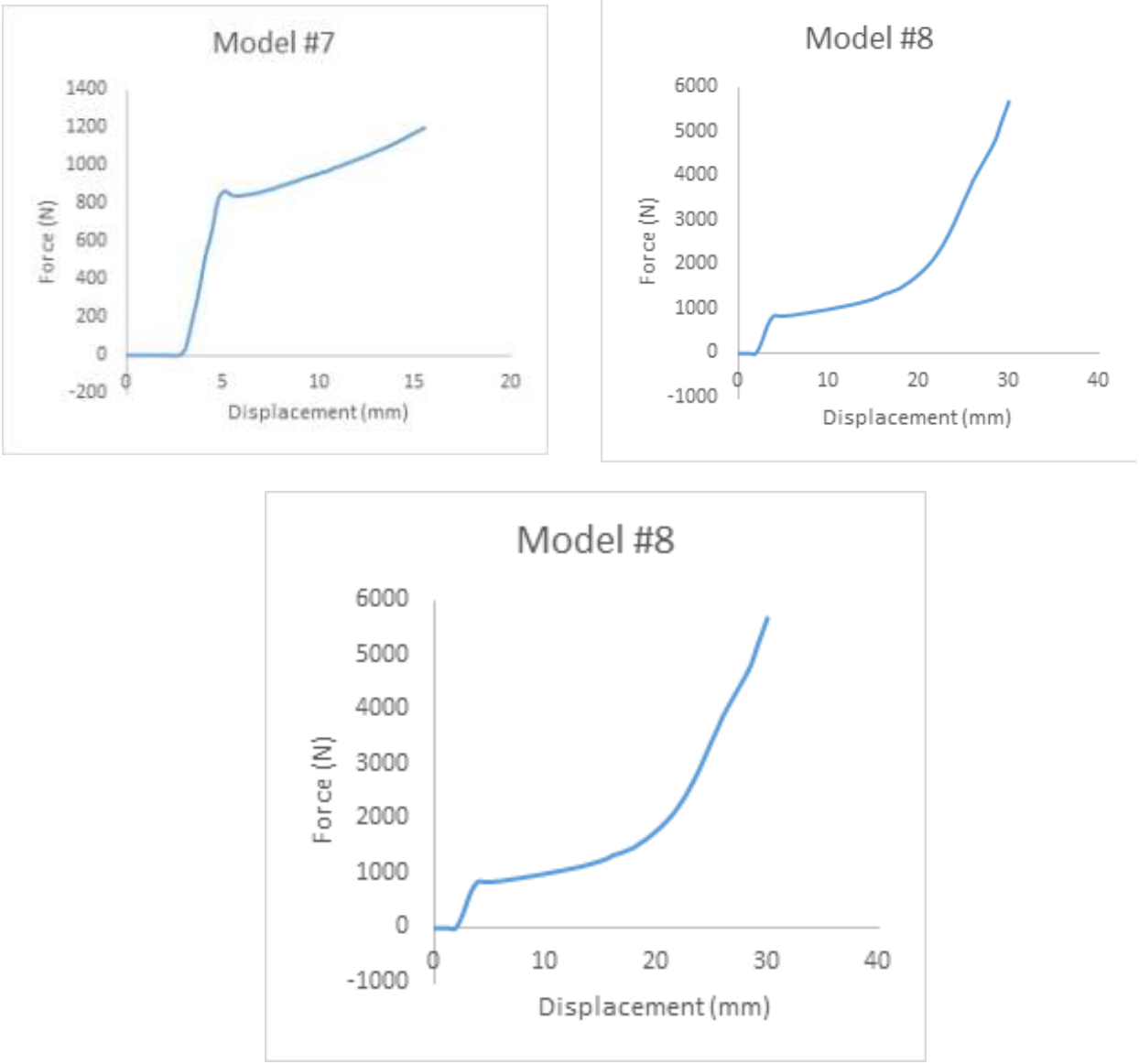

Figure 7: Load-displacement curves (a) Model 7 (b) Model 8 (c) Model 9

Energy Absorption Performance

The performance characteristics obtained upon the evaluation of energy absorption for the laminated composited from the numerical simulation are plotted in Figures (8-11). The variations in maximum crushing force Fmax was found to be significant when all the samples were compared justifying the fact that the peak crushing force is geometrically-sensitive with

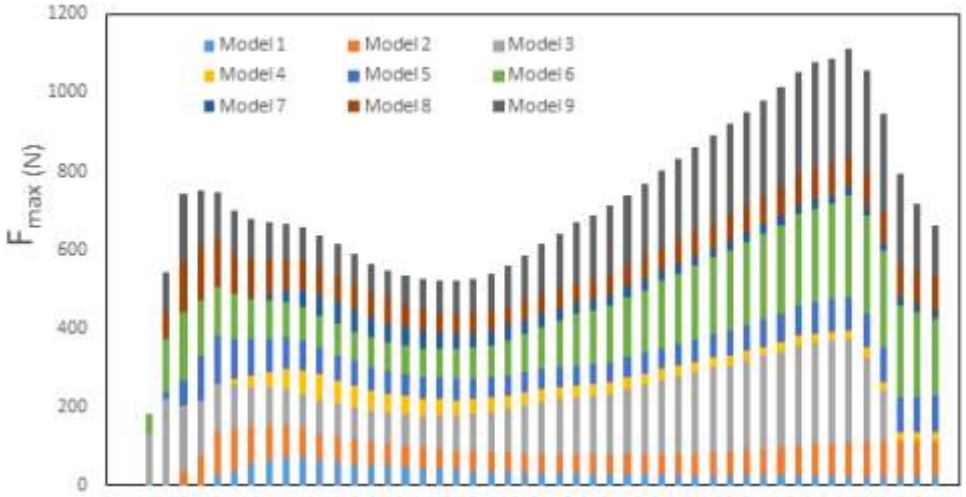

Fig. 8: Peak force (Fmax) profile for the models

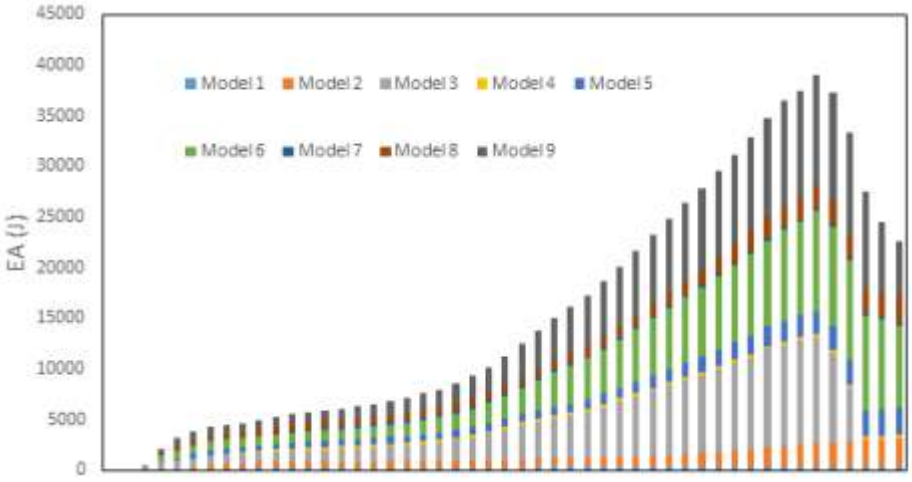

Fig. 9: Energy absorbed (EA) profile for the models

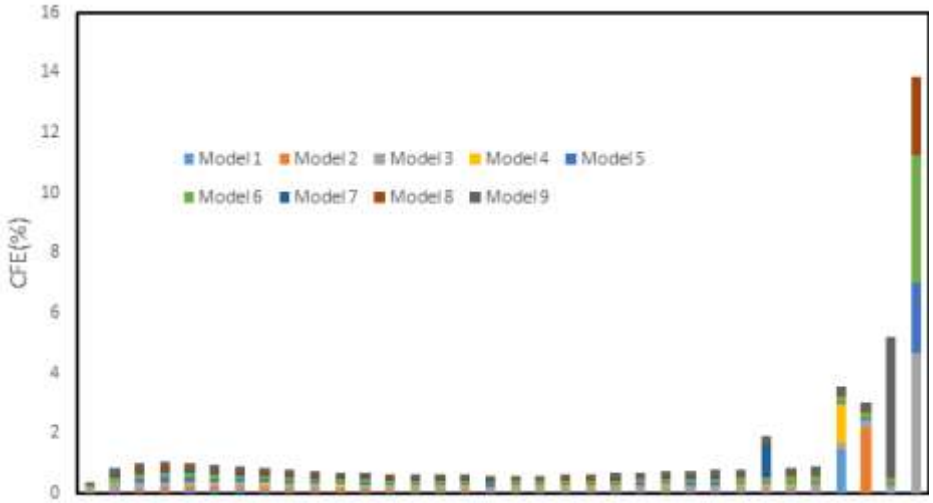

Fig. 10 Crush force efficiency (CFE) profile for the models

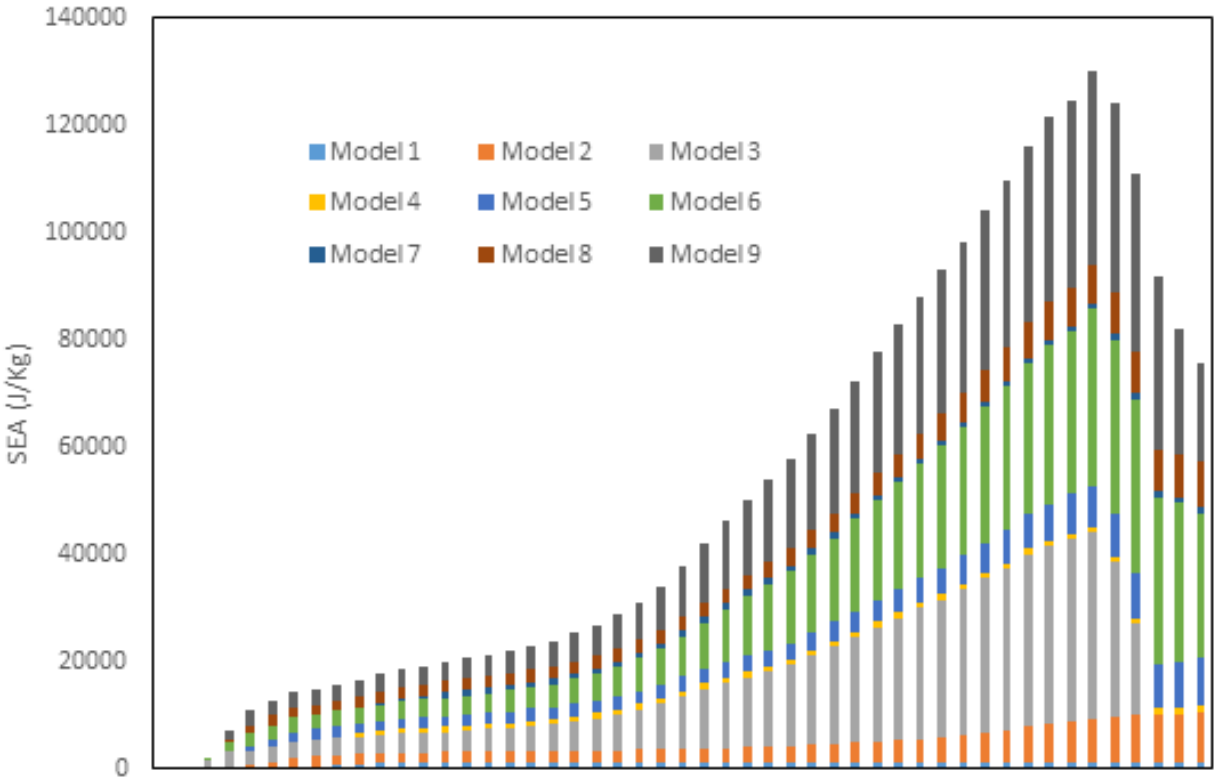

Fig. 11 Specific energy absorbed (SEA) profile for the models

respect to the evolution of volume fractions of reinforcements. Models, 7, 8 and 9 indicated the highest peak values of Fmax to indicate the capacities to restrict the incidence of high loads. Conversely, the fact that lower Fmax values were observed in Models 1 and 2 does not necessarily indicate they are the weakest models judging by the measure of stability in maintaining the peak values over the deformation history suggesting that these models could present a potential restraining capacity against sudden collapse. At certain points, models 7, 8, and 9 were characterized by a is an indication consistent with the incoherence in the interactions of the fibres with the GFRP plates. The energy absorbed, (EA) indicated that models, 9, 8 and 6 possessed the highest capacities to the absorption of loads to suggest that increasing the thickness layers significantly improves the energy absorption. However, relating this scenario with the Fmax profile, it can be suggested that a compromise needs to be achieved for optimal energy absorption because of the performance of model 8 that is composed of lower relatively lower volume fraction of fibre concentration. For the model 2, the EA increased progressively without any significant variation, and this relatively smoother profile for the composite is an indication of the superior effect of the loading rate. The foregoing scenario on the EA is also representative of the SEA. However, since crucial design criterion for lightweight structures is for the SEA values to be higher relative to a lower mass or density (Jung *et al*., 2009; Jawaid *et al*., 2019) it can be observed that the variations in SEA values followed a non-linear distribution because some composite configurations with approximate densities indicated wide disparities in their performances which crossed across the thickness variations. The SEA and CFE both are considered to represent the efficiency of EA and crashworthiness optimal performance. The higher the values indicated by these two parameters, the more impressive the energy absorption behaviors would be. Although higher SEA values were indicated for model 6, 8 and 9 in order performance, the CFE values were best for models 5, 6 and 8. Nonetheless, the SEA and CFE increased with increasing thickness of the composite tubes for a given reinforcement concentration, as more evident by the higher energy absorption reflected by model 6 of higher thickness at low volume fraction. This may be attributed to the higher stiffness effect associated with increasing thickness as it was also noticed that there exists a one-one correspondence on the increase of CFE and EA in relation to higher thickness of the GFRP plates. This performance does not necessarily have to be consistent with the requirement that associated SEA values should be correspondingly higher, it nonetheless provides a robust opportunity for a wide spectrum of design options. This anomaly may be attributed to the fact that an increase in thicknesses would increase the density which potentially increases the yield stress of the composites and consequently a higher resistance to deformation is developed as often indicated by the onset of a higher peak force. Be that as it may, a pre-

determined design criterion can therefore be deemed satisfied by a higher dissipation of energy where simultaneously a low SEA may also be acceptable. Hence, it follows that a framework to select an appropriate composite configuration that reflects the best compromise in performance characteristics for a specific optimal parameter design is feasible.

Multi objective optimization

From the parametric study of energy absorption performance, it was found that some key objective characteristics conflict with each other and it may be challenging to meet the overall engineering requirements of a structure. For example, in lightweight design considerations, structures having a large SEA values and low densities are desirable, but it has also been established that by reducing the weight of a structure in order to advance performance efficiency, the crashworthiness potential may be negatively impacted (Baykasoglu and Baykasoglu, 2017; Abbari et al, 2018). Hence, in order to achieve a critical balance of performance characteristics, the need for optimization is paramount. Regarding the composite models investigated, it was observed that the peak crush force, Pmax increased with increasing SEA values for some models while in some others, the reverse order which is the desired relationship was observed. Similar scenarios occurred in regard to the variation in CFE as well, etc. Therefore, to meet the requirements for a simultaneous optimization of any two conflicting responses, a Pareto front is determined statistically to classify the best performance through the target fitness functions generated by solving in MATLAB, the multi-objective optimization problem presented by Equation (29);

$$Q = P(x)\left\{\begin{matrix} \max SEA \ \& \ \min F_{max} \\ \max CFE \ \& \ \min F_{max} \\ s.t \\ F_{min} \le F \le F_{max} \\ T_{min} \le T \le T_{max} \end{matrix}\right\} \quad For\ all\ model\ configurations \qquad (29)$$

The optimal Pareto point Q is a set of vector of objective functions mapped from the solution P(x) of n decision variables (x_1, x_2, x_3, …..x_n). The Pareto points corresponding to optimal design characteristics are presented in Figures (12-13). The plots indicate that the SEA and CFE were found to increase with the Fmax, which is a conflicting situation from a lightweight design standpoint in the sense that for a given optimal point of the SEA and CFE against the Pmax, the corresponding values for the Pmax would be exceedingly high which runs contrary to the objective of the optimization problem.

Therefore, to achieve the best compromise in composite configuration selection that would indicate higher values of SEA and CFE relative to lower responses of the Pmax, the criterion of 'distance minimization' was applied and this is represented mathematically by Equation (30) (Baykasoglu and Baykasoglu, 2017; Abbari *et al*., 2018);

$$\min D = \left\{\sum_{i=1}^{m}[P_i^u - min(P_i)]^2\right\}^{1/2} \qquad (30)$$

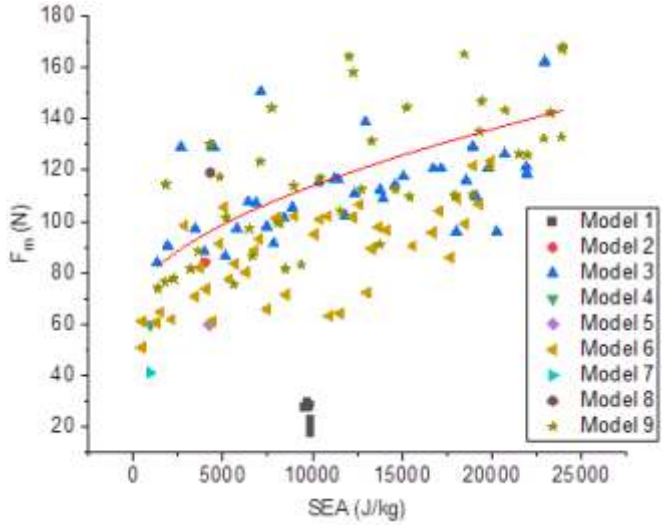

Figure 12: Pareto fronts for the models on F_m vs SEA

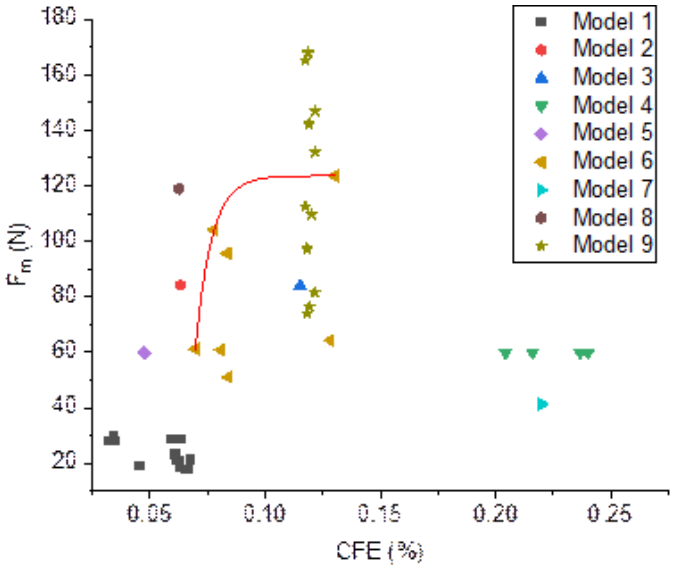

Figure 13: Pareto fronts for the models on F_m vs CFE

where *m* is the number of the objective functions (*m=2*) On the other hand, the relationship between SEA and CFE relative to density followed an expected trend which indicates a robust opportunity for the selection of wide variety of options for lightweight design. However, an accumulation of Pareto points at a specific region is observed for the SEA vs density plot, while the CFE vs density ndicated a more linear distribution of the design points. From the foregoing, composite models #2, #5, #8 and #9 were selected in consistence with the design selection criteria which is predicated on maximizing the resistance to high peak stresses, and to achieve an optimal specific energy absorption performance at minimal peak forces to satisfactorily indicate a good balance in lightweight design for crashworthiness applications.

Experimental Validation of Simulated Data

Representative models that characterized the optimal energy absorption performance based on the FEM/Genetic algorithm simulation selection criteria are shown in Figure 14. The models were subjected to quasi static testing and the observed responses are plotted in Figure 15. Evidently, it can be observed that Model 9 indicated an almost similar peak stress value of 10 MPa as compared with Model 8, which suggests these two models are objectively the best for energy absorption, however the deformation range associated with Model 8 is longer which denotes an increased capacity for energy absorption under progressive crushing. In Model 9, the incidence of transitional peaks is higher relative to Model 8 which is an indication of its weaker response to instabilities. Models #2 and #5 indicated profiles that are consistent with simulated data where

Figure 14: Samples of optimal composite laminate models for experimental validation

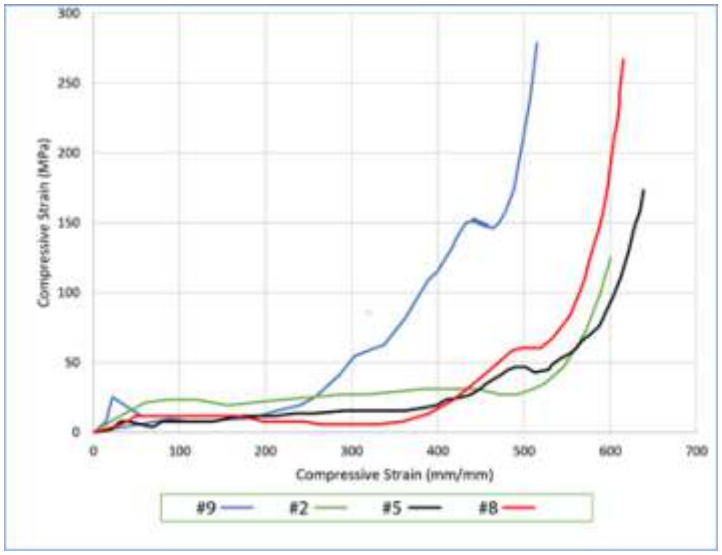

Figure 15. Experimental validation plots on optimal GFRP/coir fiber models

both of them indicated a capacity for progressive crushing at lower stresses but at the densification stage of crushing, there was a higher potential for extensional deformation by Model #5 which reasonably underscored the fact that the thickness factor is predominant over the fibre concentration in influencing the energy absorption performance. In general, the results were found to be in close agreement with the simulations.

Conclusions

The energy absorption characteristics of mesocarp coir-fibre/epoxy resin-reinforced glass fiber (GFRP) hybrid composite laminate has been investigated and the following inferences are drawn from the study;

i. As the reinforcement volume fraction increased from 40%-55%, there was a change in the deformation profile, without any rise in the initial peak forces that characterized the onset of instability due to the influence of GFRP thickness in promoting a prolonged deformation under stable crushing range during which more energy is absorbed.

ii. The behavior of the 70% mesocarp fiber reinforcement specimens, suggested that the elastic deformation domain is not sensitive to increment in reinforcement concentration, even though there is a significant change in the entire deformation profile that is facilitated by the variations in GFRP thickness.

iii. Maximum strengths were achieved for consistently thicker GFRP plates irrespective of the concentration volume of fibers. Models that indicated a range 17,000N-22,00N of maximum strength were characterized by a significant capacity to resist inhomogeneous deformation due to enhanced period of densification after progressive crushing.

iv. The energy absorbed (EA) was significant for models that indicated high resistance to peak loads and also those that indicated smoother load-unloading profiles. The specific energy absorbed (SEA) and crush force efficiency (CFE) were observed to increase with increasing GFRP thickness for a given reinforcement concentration across the models.

v. By genetic algorithm, models #2, #5, #8 and #9 were found to be most consistent with the design selection criterion predicated on maximizing the resistance to high peak stresses for an optimal specific energy absorption performance, and these results were correspondingly in close agreement with the simulations by experimental validation.

References

Abbari, M., Reddy, S., Ghafari-Nazari, A. and Fard, M. (2018). Multiobjective crashworthiness optimization of multi-cornered thin-walled sheet metal members, *Thin-walled Structures 89*, 31-41.

Abolfathi, M. and Nia, A. (2018). Optimization of energy absorption properties of thin-walled tubes with combined deformation of folding and circumferential expansion under axial load. Thin-walled structures 130, 57-70.

Abood, I., Odaa, S., Hasan, K. and Jasim, M. (2021). Properties evaluation of fiber reinforced polymers and their constituent materials used in structures- A review; Materi

als today: Proceedings 43, (2), 1003-1008.Abramowicz, W. and Jones, N. (1986). Dynamic progressive buckling of circular and square tubes, Int. *Journal of Impact Engineering,* 4, 243-270.

Albahash, Z. and Ansari, M. (2017). Investigation on energy absorption of natural and hybrid fiber under axial static crushing. *Composite Science Technology,* 151, 52-61.

Alshahrani, H., Sebaey, T., Allah, M. and El-Baky, M. (2022). Quasi-static axial crushing performance of thin-walled tubes with circular discontinuities, *Journal of Composite Materials* 56 (27), 4195-4218.

Baroutaji, A., Sajjia, M. and Olabi, A. (2017). On the crashworthiness performance of thin-walled energy absorbers: Recent advances and future developments, *Thin-walled Structures 118,* 137-163.

Baykasoglu, A. and Baykasoglu, C. (2017), Multiple objective crashworthiness optimization of circular tubes with frictional-graded thickness via artificial neural networks and genetic algorithms. *Proc. Inst. Mech. Eng Part C: J Mech Eng Sci. 231*.

Beardmore, P. and Johnson, C. (1986). The potential for composites in structural automotive applications, *Journal of Composite Science and Technology 26 (4),* 251-281.

Benveniste, Y. (1987). A new approach to the application of Mori-Tanaka's theory in composite materials, *Mechanics of Materials 6* (2), 147-157.

Cai, Z., Wang, D., Smith, S. and Wang, Z. (2016). Experimental investigation on the seismic performance of GFRP-wrapped thin-walled steel tube confined RC column, *Engineering Structures 110*, 269-280.

Camanho, P. and Davila, C. (2002). Mixed mode decohession finite element for the simulation of delamination in composite materials. *Tech Rep NASA/TM-2002-211737.*

Esnaola, A., Tena, I., Aurrekoetxea, J., Gallego, I. and Ulacia, I. (2016). Effect of fiber fraction on energy absorption capabilities of E-glass/polyester automotive crash structures, *Composites Part B: Engineering, 85*, 1-7.

Essabir, H., Bensalah, M., Rodrigue, D., Doulifid, R. and Qaiss, A. (2016). A structural mechanical and thermal properties of bio-based hybrid composites from waste coin residues: fibers and shell particles. *Mechanics of Materials 93*, 134-144.

Farley, G. (1987). Energy-absorption capability of square cross section composite tube specimens, United States Department of the Army.

Hashin, Z. (1980). Failure criteria for uni-directional fiber composites. *Journal of Applied Mechanics, 47* (6), 329-334.

Issac, C. and Ezekwem, C. (2021). A review of the crashworthiness performance of energy absorbing structures within the context of materials, manufacturing and maintenance for sustainability, *Composite Structures 257*, 113081.

Jawaid, M., Thariq, M. and Saba, N. (2019). Mechanical and physical testing of bio-composites, fiber-reinforced composite and hybrid composites, *Woodhead Publishing*, United Kingdom, 43-57.

Jung, D., Kim, H. and Choi, N. (2009). Aluminum-GFRP hybrid square tube beam reinforced by a thin composite skin layer, *Composites: Part A 40*, 1558-1565.

Kathiresan, M., Manisekar, K. and Manikandan, V. (2014). Crashworthiness analysis of glass fibre/epoxy laminated thin walled composite conical frusta under axial compression, *Composite Structures 108*, 584-599.

Liu, X., Belkassem, B., Jonet, A., Lecompte, D., Hemelrijck, D., Pintelon, R. and Pyl, L. (2019). Experimental investigation of energy absorption of circular carbon/epoxy composite tubes under quasi-static and dynamic crush loading, *Composite Structures, 227*, 111266.

Omairey, S., Dunning, P. and Sriramula (2018). Development of an ABAQUS plugin tool for periodic RVE homogenization, *Engineering with Computers, 35*, 567-577.

Paz, J., Diaz,J., Romera, L. and Costas, M. (2014). Crushing analysis and multi-objective crashworthiness optimization of GFRP honeycomb-filled energy absorption devices, *Finite Elements in Analysis and Design 91*, 30-39.

Pickering, K., Efendy, M. and Le, T. (2016). A review of recent developments in natural fibre composites and their mechanical performance, *Composites: Part A 83*, 98-112.

Pickett, L. and Dayal, V. (2012). Effect of tube geometry and ply-angle on energy absorption of a circular glass/epoxy crush tube- a numerical study, *Composites Part B: Engineering, 43*, (8), 2960-2967.

Safri, S., Sultan, M., Jawaid, M. and Jayakwrishna, K. (2017). Impact behavior of hybrid composite for structural applications: A Review, *Composite Part B* 133, 112-121.

Sebaey, T., Junaedi, H., Alshahrani, H., Alyahmani, R. and Akkad, K. (2023). Effect of thermal aging on the crashworthiness of foam-filled CFRP composite tubes under lateral compression, *Journal of Materials Research and Technology, 23*, 1-12.

Sengupta, S. and Basu, G. (2016). Properties of coconut fiber. *Reference Module in Material Science and Material Engineering*, Encyclopedia of Renewable and Sustainable Materials, 2, 263-281.

Sun, G., Guo, X., Li, S., Ruan, D. and Li, Q. (2020). Comparative study for aluminum/ GFRP/ CFRP tubes for oblique lateral crushing, *Thin-walled Structures 152*, 106420.

Sun, G., Wang, Z., Hong, J., Song, K. and Li, Q. (2018). Experimental investigation of the quasi-static axial crushing behavior of filament-wound CFRP and aluminum/CFRP hybrid tubes, *Composite Structures, 194*, 208-225.

Supian, A., Supian, S., Zhuhri, M., Zainudin, E. and Ya, H. (2019). Crashworthiness performance of hybrid kenaf/glass fibre reinforced epoxy tube on winding orientation effect under quasi-static compression load, *Defense Technology 16*, (5) 1051-1061.

Weirzbicki, T. and Abramowicz, W. (1983). On the crushing mechanism of thin-walled structures. *Journal of Applied Mechanics, 50* (4), 727-734.

Wu, Q. and Zhi, X. (2020). Experimental and numerical study of GFRP-reinforced circular steel tube under axial compression, *Journal of Constructional Steel Research 168*, 105990.

Xiang, X., Lu, G., Li, Z. and Lv, Y. (2018). Large deformation of tubes under oblique lateral crushing, *International Journal of Impact Eng., 110*, 138-148.

Zhang, J., Ouyang, Q; Guo, Q., Li, Z., Fan, G., Su, Y., Jiang, L., Lavernia, E., Schoenung, J., and Zhang, D. (2016). 3D microstructure-based finite element modelling of deformation and fracture of SiCp/Al composites, *Composites Science and Technology 123*, 1-9.